Dynamic cross-correlations between entangled biofilaments as they diffuse

Boyce Tsang[a,1], Zachary E. Dell[a,1], Lingxiang Jiang[b,1], Kenneth S. Schweizer[c,d], and Steve Granick[e,2]

[a]Department of Physics, University of Illinois at Urbana–Champaign, Urbana, IL 61801; [b]Department of Materials Science and Engineering, Jinan University, Guangzhou 510632, China; [c]Department of Materials Science, University of Illinois at Urbana–Champaign, Urbana, IL 61801; [d]Department of Chemistry, University of Illinois at Urbana–Champaign, Urbana, IL 61801; and [e]IBS Center for Soft and Living Matter, Ulsan National Institute of Science and Technology, Ulju-gun, Ulsan 689-789, South Korea

Contributed by Steve Granick, February 7, 2017 (sent for review December 20, 2016; reviewed by Marina G. Guenza and Eric R. Weeks)

Entanglement in polymer and biological physics involves a state in which linear interthreaded macromolecules in isotropic liquids diffuse in a spatially anisotropic manner beyond a characteristic mesoscopic time and length scale (tube diameter). The physical reason is that linear macromolecules become transiently localized in directions transverse to their backbone but diffuse with relative ease parallel to it. Within the resulting broad spectrum of relaxation times there is an extended period before the longest relaxation time when filaments occupy a time-averaged cylindrical space of near-constant density. Here we show its implication with experiments based on fluorescence tracking of dilutely labeled macromolecules. The entangled pairs of aqueous F-actin biofilaments diffuse with separation-dependent dynamic cross-correlations that exceed those expected from continuum hydrodynamics up to strikingly large spatial distances of ≈15 μm, which is more than 10^4 times the size of the solvent water molecules in which they are dissolved, and is more than 50 times the dynamic tube diameter, but is almost equal to the filament length. Modeling this entangled system as a collection of rigid rods, we present a statistical mechanical theory that predicts these long-range dynamic correlations as an emergent consequence of an effective long-range interpolymer repulsion due to the de Gennes correlation hole, which is a combined consequence of chain connectivity and uncrossability. The key physical assumption needed to make theory and experiment agree is that solutions of entangled biofilaments localized in tubes that are effectively dynamically incompressible over the relevant intermediate time and length scales.

entangled | cross-correlation | biofilament | reptation | imaging

The long-standing quest to understand why the mobility of entangled linear polymers is ultraslow normally considers the diffusion of a single average macromolecule in its average surrounding environment, most prominently envisioned as a polymer reptating through the confining Edwards–de Gennes tube composed of the identical polymers that surround it (1–6). Although differing in important respects according to polymer geometry (e.g., flexible and semiflexible chains, rigid rods, and branched polymers), all share the peculiarity that because the size of the macromolecule vastly exceeds the size of individual units along it, adjoining segments on a tagged polymer become correlated over large separations simply because they are covalently bonded and cannot cross other macromolecules. In this paper, our focus is not on the familiar single-polymer problem (1–13) but rather on the open question of how the motion of a given reptating macromolecule is coupled in space and time with others that reptate within its pervaded volume. The fractal and strongly interpenetrating nature of linear polymers in dense liquids causes the number of "correlated neighbors" on the macromolecular length scale to grow strongly as the polymer size increases (1–3, 14). The dynamical consequences of such a feature are not addressed by the classical reptation-tube model, which ignores the correlated motion of neighboring polymers, for simplicity and perceived intractability (1–6). Analysis of the latter involves crowding effects far beyond the nearest-neighbor cage scale central to understanding slow dynamics in small molecule and colloidal liquids (15–18).

We focus on intermediate time and length scales when the system mechanically is a soft solid showing an emergent dynamic plateau modulus due to polymer localization in two transverse spatial directions, yet the individual constituents continue to display the Fickian diffusion of a viscous liquid in the direction of the polymer contour (1–3, 9). The archetypal textbook static representation (1–3) of a concentrated polymer solution is threadlike polymers of contour length L separated by the average "mesh" distance ξ_m between neighboring strands, with time and length scales summarized in Fig. 1*A* for stiff filaments. On intermediate scales, polymers remain entangled and slowly diffuse in the longitudinal direction but are dynamically equilibrated (localized) in their tubes, resulting in a near-constant time-averaged density as indicated by the "fat cylindrical tubes" depicted in Fig. 1*B*.

One focus of our work is to understand the coordinated motion of entangled polymers. The hydrodynamic continuum limit of the pair or relative two-polymer diffusion coefficient is known to have correlations that decay as $1/r$, where r is separation (19–26). Our experimental measurements cross over to this scaling at large separation but earlier they deviate upward from this prediction, suggesting conclusions about the respective importance of hydrodynamic and nonhydrodynamic correlations as a function of length scale (Fig. 1*C*). This is relevant for understanding the lower bound of distance beyond which applicability of the two-point microrheology technique is predicated (20–24). It is also relevant to cytoskeletal dynamics of stiff biofilaments such as actin and microtubules and potentially to the "crowding"

Significance

Highly entangled biofilaments are ubiquitous in the cytoskeleton and present a paradigm in polymer physics and biophysics. Here, rather than conventionally seeking to understand the self-diffusion of a single tagged entangled polymer we inquire into dynamic cross-correlations between nearby filaments as they diffuse anisotropically in aqueous solution. Our combined fluorescence tracking experiments and statistical mechanical modeling show that the continuum limit is reached only at distances beyond the filament length, in this system beyond the large distance of ≈15 μm. This noncontinuum behavior at micron-scale distance may be related to the "crowding" problem in biological function.

Author contributions: B.T., Z.E.D., L.J., K.S.S., and S.G. designed research; B.T., Z.E.D., L.J., and K.S.S. performed research; B.T., Z.E.D., L.J., K.S.S., and S.G. analyzed data; and B.T., Z.E.D., L.J., K.S.S., and S.G. wrote the paper.

Reviewers: M.G.G., University of Oregon; and E.R.W., Emory University.

The authors declare no conflict of interest.

Freely available online through the PNAS open access option.

[1]B.T., Z.E.D., and L.J. contributed equally to this work.

[2]To whom correspondence should be addressed. Email: sgranick@illinois.edu.

This article contains supporting information online at www.pnas.org/lookup/suppl/doi:10.1073/pnas.1620935114/-/DCSupplemental.

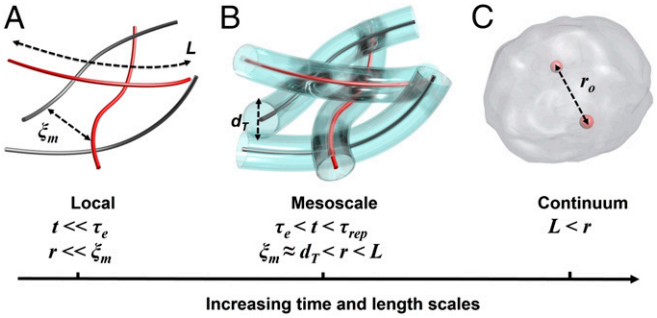

Fig. 1. Schematic illustration of the space–time regimes considered in this study. (*A*) At times less than the entanglement onset time τ_e and lengths less than the static geometric mesh length ξ_m, entangled macromolecular filaments behave as thin, dilute, weakly bending threads of length L and diameter b that experience solvent-mediated hydrodynamic interactions, whereas (*B*) At times longer than τ_e but less than the reptation time τ_{rep}, and distances intermediate between the mesh or tube diameter and polymer contour length, the filaments are effectively densely packed, filling at a nearly constant average density a tube of diameter d_T, and they reptate along their contours with diffusion constant $D_{//}$. Interfilament hydrodynamic forces are screened on these intermediate length scales. (*C*) The very large distance structureless continuum limit considered by traditional mechanics and hydrodynamics, in which the relative motion of two probes is considered as a function of time and their separation r_0.

problem in biological function (11–13, 27–30). Generic for all fluids of interpenetrating, entangled macromolecules, thematically this matter can also be explored in flexible random coil polymer solutions and melts in addition to the biofilaments considered in this paper, although we do not do so here.

Biopolymer filaments of F-actin in aqueous solution present an attractive test bed for theory and experiment to address this matter (9, 23, 31, 32). They are globally isotropic yet heavily entangled at the concentrations studied here. The intermediate time-scale regime of anisotropic diffusion, which is longer than the entanglement onset time ($\tau_e \sim 10^{-1}$ s) (31) to equilibrate within a tube but far less than the terminal flow or reptation time ($\tau_{rep} \sim 10^3$ s) (31, 32), is experimentally accessible. The time and length scales we probe, and a cartoon of the system, are summarized in Fig. 2 *A* and *B*. The experimental system is complicated by the fact that actin length (L) distribution from this method of sample preparation is polydisperse (7, 9), so it is reassuring that our calculations described below find insensitivity to both the magnitude of L and its polydispersity over the range relevant to experiment. The geometric mesh size ($\xi_m \sim 0.1$ μm, the average distance between filament crossing points) and the tube diameter ($d_T \approx \xi_m$, a dynamical scale relevant to the emergent soft elasticity) are one to two orders of magnitude less than the mean filament length but orders of magnitude larger than the solvent water molecules ($d \sim 0.3$ nm) and filament thickness ($b \sim 8$ nm) (7, 9). The persistence length is large, ~17 μm, so for diffusive transport it is reasonable to consider these stiff filaments as almost rod-like (9). The theoretical calculations have used $L = 15$ μm, the same order of magnitude as the mean filament length, except when otherwise stated.

Experimentally, this work combines fluorescence imaging techniques pioneered by Sackmann and coworkers (9), whose spatial resolution is diffraction-limited, with subdiffraction-resolution imaging of sparsely labeled elements of these same actin filaments. We find the system is globally isotropic for the F-actin concentrations (c is mass fraction) studied, 0.5, 1.0, and 2.0 mg/mL (Fig. 2*B*). Relative to the critical entanglement concentration, $c_e \approx 0.4$ mg/mL (31, 32), these systems are highly entangled, with c/c_e in the range 1 to 5. One fluorescent dye labels the chain backbone uniformly and hence its emission is diffraction-limited, whereas the chain is also labeled in sparse abundance with a second fluorescent dye to give subdiffraction resolution. We screen the data to find filaments in close proximity that both lie within the focal plane so that the distance between segments on them can be drawn in 2D with confidence (Fig. 2*C*). In parallel, local displacements of each filament are visualized with subdiffraction resolution by inspecting the second dye of such sparse abundance that they serve as point sources with a peak emission that can be quantified with nanometer precision (Fig. 2*C*) (33, 34). Earlier we introduced the technique of sparse labeling, which makes this possible (7), but here we apply it to the problem of correlated dynamics. The time dependence of relative displacement between points on neighboring filaments, each of them localized with nanometer resolution, is then inspected (Fig. 2*D*). Appearing in epifluorescence microscope images as circular spots, centroid tracking of their positions gave a precision of ±20 nm over times as short as 50 ms.

Recently we reported a statistical mechanical theory to describe intermediate-scale space–time correlations between diffusing spherical colloids in dense quasi-2D suspensions based on interparticle frictional effects and effective structural forces, and its

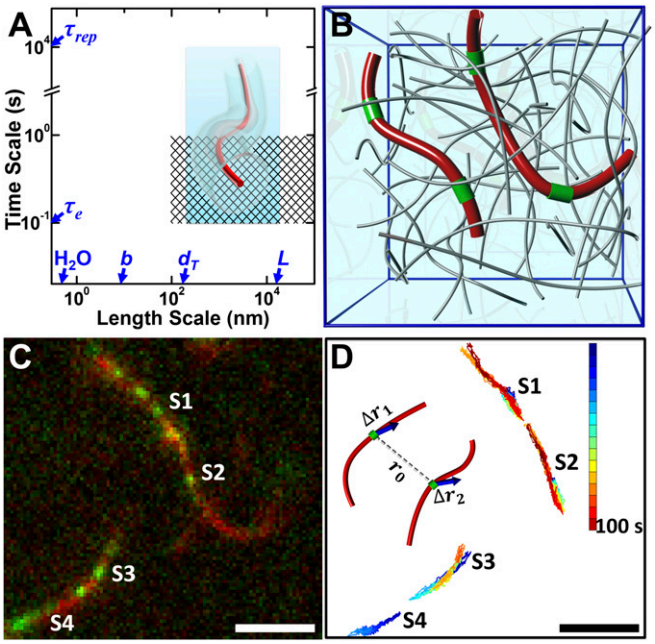

Fig. 2. Experimental setup in which point fluorescence sources of neighboring entangled filaments are tracked over time scales far less than the disentanglement time. Cross-correlated diffusion of actin filaments in isotropic aqueous solution is quantified using fluorescence tracking. (*A*) The relevant time scales (lower bound τ_e, upper bound τ_{rep}) and length scales (b is the filament diameter, d_T the tube diameter, and L the filament contour length). The intermediate time and length scale regime of present interest is highlighted by cyan, and the experimental accessible regime is denoted by the cross pattern. (*B*) Three-dimensional schematic representation of the experimental setup. We consider entangled solutions in which a tracer quantity of actin filaments labeled with fluorescent dyes of two colors is mixed with an excess of filaments of the same kind except that they are unlabeled. Red traces the filament contour. Green represents sparse labeling to provide point sources of fluorescence whose relative displacements are evaluated with nm precision as time elapses. (*C*) After screening datasets to find the rare cases when neighboring filaments both lie in the 2D focal plane, the time-dependent diffusion of red and green colors false-colored is tracked parallel to and transverse to the line between them at numerous separations r_0. In these raw data, green positions S1 and S2 on one molecule are cross-correlated relative to green positions S3 and S4 on the other molecule. (*D*) Image processing eliminates the background fluorescence and generates experimentally the time-dependent mutual trajectories of point sources S1, S2, S3, and S4 on the two molecules. They are traced against time with color coding up to 100 s shown on the right while calculating the scalar distance r_0 between small measured vector displacements Δr_1 and Δr_2 of neighboring filaments. (Scale bars: 4 μm.)

predictions compare favorably to experiments with colloids (35). Here, we qualitatively extend this approach to the more complex case of entangled biopolymers and compare its predictions to our experiments to quantify nonhydrodynamic, noncontinuum cross-correlations in long-range pair diffusion and test the proposed mechanism. Although hydrodynamics is crucial at very short and very long distances, it is screened on the intermediate length scales of primary interest here ($\xi_m < r < L$ per Fig. 1) due to polymer interpenetration (25, 26). Hence, the observed correlated motion is ascribed to a nonhydrodynamic origin. For the final cross-over to continuum behavior, our experimental results are in agreement with two-point microrheology measurements (22, 23).

Experimental Results

The geometric mesh length of F-actin solutions is $\xi_m = \sqrt{9/\rho_r L} = (280\,\text{nm})(c[\text{mg/mL}])^{-1/2} \approx 200-400$ nm (ρ_r is filament number density, where L is the contour length and the dynamic tube diameter $d_T = (180\text{ nm})\ (c[\text{mg/mL}])^{-3/5} \approx 120-280$ nm. These lengths are mesoscopic (36, 37) but far smaller than filament length for all concentrations studied. The experimental times probed (Fig. 2*A*) are longer than required for dynamic equilibration of a filament in its tube but far below the reptation time (31, 32). Fig. 2 *C* and *D* illustrates the joint detection of the filament contour and sparse point sources along it.

To validate the credibility of our experimental measurements, first we confirm the known phenomenon that these filaments diffuse preferentially parallel to their contour (i.e., by reptation). The mean-square displacements (MSD) quantified with nanometer-level accuracy using sparse labeling were measured and plotted against time on log-log scales in Fig. 3*A*. Discriminating in this way their time-dependent position fluctuations transverse ($\perp$) and parallel (//) to the filament backbone at 1 mg/mL concentration, the transverse displacements are found to be highly subdiffusive, indicating strong transverse localization. The residual slight increase of MSD with time (MSD $\sim t^{0.2}$ empirically) likely reflects limited motions such as contour length fluctuation (2). In contrast, the parallel displacements are close to linear in elapsed time (MSD $\sim t^{0.9}$ empirically), from which the implied diffusion constant is $D_{//} \approx 0.1\ \mu\text{m}^2/\text{s}$ for all three concentrations that were studied. Importantly, this value is almost identical to the hydrodynamics-determined polymer diffusion constant in dilute solution, in good agreement with the reptation-tube model of entangled rods (1–3, 38).

Per Fig. 2*D*, the space–time relative displacement correlation function, $C_{rr}(r_0;t)$, is defined as the correlated displacements of two tagged segments on different filaments as a function of their initial separation r_0 and elapsed time t during which thermal motion causes displacement amplitudes that are modest relative to r_0:

$$C_{rr}(r_0;t) \equiv \left\langle \Delta r_{1,r}(t)\Delta r_{2,r}(t)\right\rangle_{r_0}, \quad [1]$$

where $\Delta\vec{r}_\alpha(t) = \vec{R}_\alpha(t) - \vec{R}_\alpha(0)$ is the vector displacement of segment α in a time t relative to its initial position, and the subscript r corresponds to projection along the initial separation vector of the two tagged segments. The symbol $\langle\ldots\rangle_{r_0}$ indicates that the ensemble average is performed at fixed segment separation r_0. Fig. 3*B* plots $C_{rr}(r_0;t)$ for c = 0.5 mg/mL (main frame) and c = 2.0 mg/mL (inset) at elapsed times 0.1, 0.2, and 0.4 s. The observation that these correlations are approximately proportional to the lag time regardless of concentration suggests physically that the elementary kinetic process dominating displacement correlation is filament reptation, so it is meaningful to infer a spatially dependent relative diffusion constant, $D_{rr}(r_0) = C_{rr}(r_0,t)/t$. In Fig. 4*A* D_{rr} is plotted against intersegment separation. The satisfactory data collapse for all elapsed times at fixed filament concentration further supports the physical interpretation that pair dynamics evolve in a Fickian fashion. When one considers that the dynamical structure is expected to depend weakly on concentration (because for the concentration studied $\xi_m/d_T \propto c^{-1/10}$ theoretically) (36, 37), it is pleasing to confirm that D_{rr} is insensitive to concentration over the range that we studied.

When particles interact via conservative central forces, it is natural to expect radial correlations (D_{rr}) to dominate over transverse (D_{tt}) correlations for a nonhydrodynamic mechanism (35). Testing this proposition, our experiments indeed find that $D_{tt} << D_{rr}$ on intermediate length scales less than the filament length (Fig. S1), further supporting the idea that a nonhydrodynamic

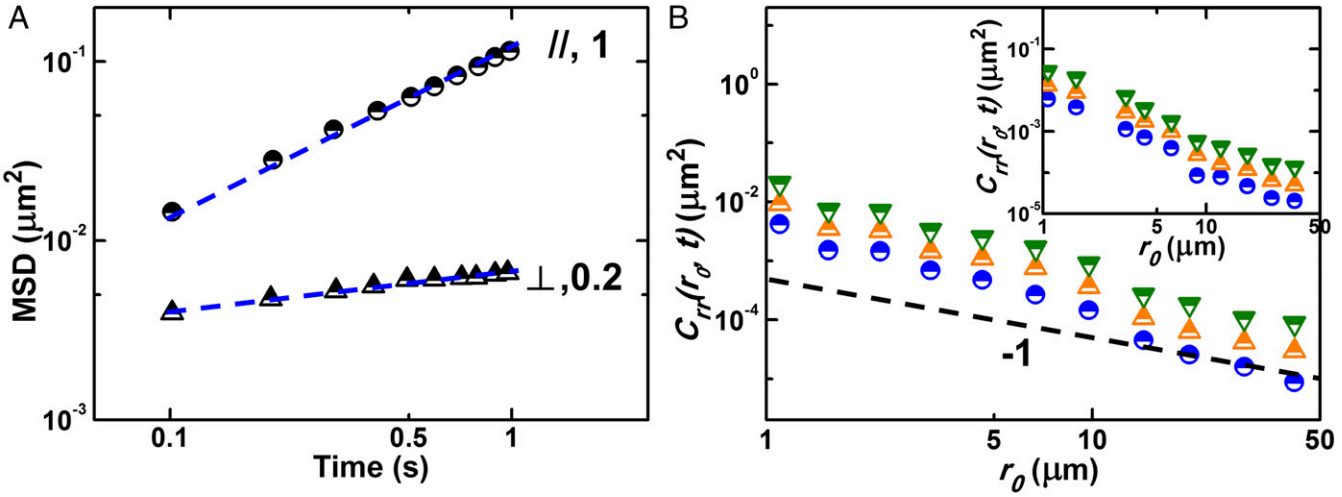

Fig. 3. Experimental Results. (*A*) MSD from points of sparse labeling is plotted against time on log-log scales. The experiments agree with the reptation model, diffusion is in the direction of the filament contour, being consistent with slope 1.0 and $D// = 0.13\ \mu\text{m}^2\cdot\text{s}^{-1}$, whereas perpendicular to the filament backbone the experimentally measured slope on this time scale is far less (phenomenologically it is 0.2), showing that diffusion in this direction is almost completely localized. For these two representative trajectories (open symbols and filled symbols) the filament backbone is at concentration 1 mg/mL. (*B*) From data of the kind summarized in Fig. 2*D* cross-correlations between neighboring filaments were quantified. Here, ensemble-averaged displacement correlations $C_{rr}(t)$ between tagged segments are plotted at times 0.1 s (circles), 0.2 s (upright triangles), and 0.4 s (inverted triangles). The main frame and inset show 0.5- and 2-mg/mL actin samples, respectively.

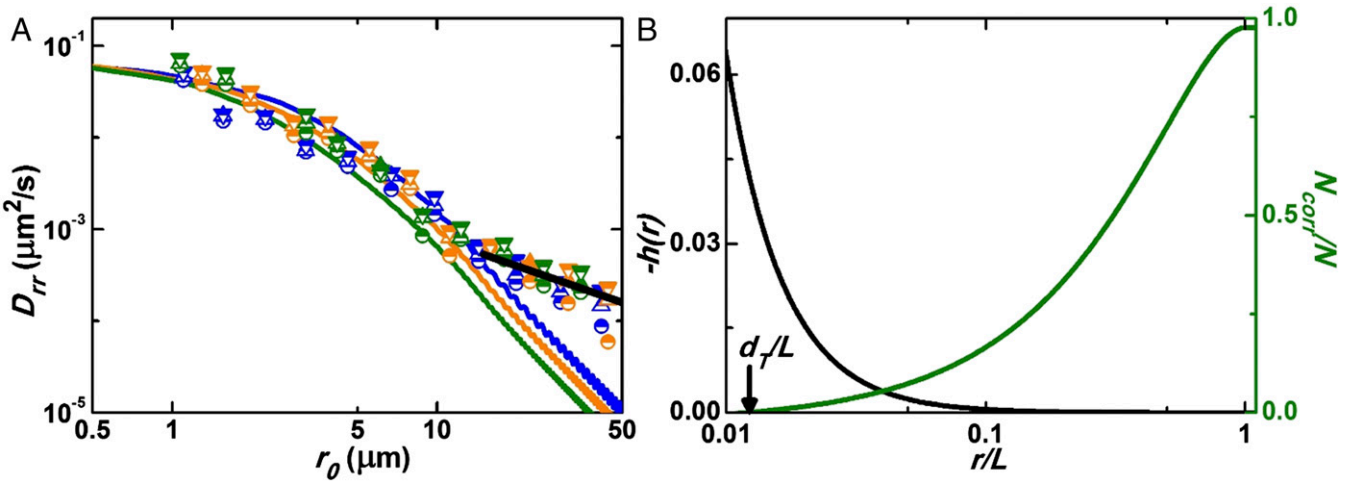

Fig. 4. Experimental results for the separation-dependent relative diffusivity and comparison with theoretical predictions. (*A*) On log-log scales the relative diffusivity data are plotted as points against separation for the actin concentrations 0.5 mg/mL (blue), 1 mg/mL (yellow), and 2 mg/mL (green) and times 0.1 s (circles), 0.2 s (upright triangles), and 0.4 s (inverted triangles). The solid curves show the corresponding theoretical predictions for the actin concentrations 0.5 (blue), 1 (yellow), and 2 (green) mg/mL and $L = 15$ μm. The straight line with slope −1 is the continuum hydrodynamic prediction. (*B*) On the left ordinate axis, the nonrandom part of the intersegment pair distribution function, $h(r)$, is plotted against logarithmic normalized separation r/L for monodisperse, thin, rigid rods of length $L = 15$ μm at fixed concentration $c = 1$ mg/mL. On the right ordinate axis, the metric of the number of spatially correlated segments on different rods in a spherical region of radius r centered on a tagged segment, divided by total number of segments N, is plotted against logarithmic r/L. The tube diameter relative to L (d_T/L) is identified for reference.

mechanism is dominant on intermediate length scales. This differs qualitatively from the continuum hydrodynamic-based expectation that the magnitudes of radial and transverse displacement correlations should be comparable (22, 23).

Consider now the extremes of small and large separation between segments on different filaments. The smaller the separation between tagged segments, the fewer other filament segments reside between them, so physically one would anticipate that on length scales less than the physical mesh the viscous drag will approach that experienced by a single filament. Consistent with this, we find experimentally that $D_{rr} \approx D_{\|}$ in the limit of the smallest resolvable separations. However, the continuum hydrodynamics is expected to be recovered in the limit of large separations with $D_{rr} \propto 1/r_0$ (19). Such expectation was confirmed by prior two-point microrheology measurements (20–24), although it is true that the microrheology community has used the different approach of using tracer beads to detect relative displacement, not our approach of sparsely labeled, fluorescently tagged filaments. Literature measurements of the bulk viscoelastic loss modulus of heavily entangled F-actin solutions (no probe particles) at frequencies of ∼1–10 Hz (relevant to the time scales of our experiments) find that $G''(\omega)/\omega$ is roughly constant. This allows an effective viscosity to be extracted, and we deduce $\eta_{eff} \sim (50-100)\eta_0$, where η_0 is the viscosity of water (39, 40). Fig. 4*A* shows that the heuristic proposition that $r_0 D_{rr}^{HD}(r_0) = k_B T/(2\pi\eta_{eff})$ in the $r_0 >> L$ hydrodynamic regime describes our data with a value $\eta_{eff} = 82\ cP \approx 90\ \eta_0$ consistent with its independent estimate. Microrheology measurements (22, 23) in actin solutions have also been performed with probe particles separated by more than 10 μm and at frequencies relevant to our measurements. They find a weakly frequency-dependent $D_{rr} r_0 \approx$ 0.003–0.01 μm³/s (22, 23), which again leads to a physically reasonable value of the effective viscosity ∼50–100 times that of water. Moreover, the data in Fig. 4*A* are consistent with a $1/r_0$ decay but only for separations larger than roughly the filament length and with a value of $D_{rr} r_0 \approx 0.008$ μm³/s.

This experimental puzzle that continuum-based hydrodynamics seems to apply only beyond such large separations motivated the theoretical work that follows. It is known that at distances of order the mesh size and times below the reptation time, polymers appear as effectively fixed obstacles that "scatter" or "screen" the solvent flow field, as was articulated long ago by Doi, Edwards, and others (2, 25, 26), so we explore the consequences.

Theory and Discussion

Our vision of the physical situation is sketched in Fig. 1. The relevant length scales of the entangled F-actin solution suggest the emergence of a dynamic structure (Fig. 1*B*) corresponding to gently bending "cylindrical fat tubes" of mean thickness the tube diameter (d_T), with an actin density that is roughly uniformly smeared inside the tube region on intermediate time scales. Importantly, because the mesh size and tube diameter nearly coincide in this semiflexible F-actin system, the tubes are densely packed and in repulsive contact (3, 36, 37). These features physically suggest a model based on "dynamic incompressibility" (small collective density fluctuations) being applicable on intermediate time and distance scales.

The problem now becomes how to understand the emergent intermolecular dynamical correlations between pairs of filaments associated with their diffusive reptation motion. The ideas described below are based on modeling biopolymer filaments as rigid rods, which for the interfilament dynamics associated with longitudinal reptation should be a reliable simplification. To formulate the theoretical model for correlated two-filament diffusion, we consider the connection between effective entropic forces and collective structure of the entangled fluid on time and length scales beyond which each polymer has equilibrated within its tube in a region of space. Effective incompressibility implies the emergence of a strong interpolymer spatial correlation known as the de Gennes "correlation hole" (2, 3) and an effective long-range repulsion that can induce space–time dynamic displacement correlations. We formulate this physical picture using quantitative statistical mechanics by combining the reptation-tube ideas of single polymer motion (4–6) with force-level generalized Brownian motion ideas for predicting intermolecular dynamical correlations (35, 41–46). Here we sketch the essential elements of the model and theory and present technical details in *Supporting Information*.

As successfully implemented in recent theoretical studies of Stokes–Einstein violation of nanoparticles in polymer melts (47) and dynamic displacement correlations in dense colloidal fluids (35), the total pair diffusivity is estimated as the sum of

independent hydrodynamic and nonhydrodynamic contributions, $D_{rr} = D_{rr}^{HD} + D_{rr}^{non-HD}$, over the experimentally accessible length scale, $\xi_m \sim d_T < r < 10L$. We further assume that hydrodynamics is a second-order effect (thus $D_{rr} \approx D_{rr}^{non-HD}$) on the intermediate distance regime of most interest, $\xi_m < r < L$, for two reasons: Solvent-mediated hydrodynamic forces are exponentially screened, as is well known from prior experimental and theoretical studies (2, 25, 26), and our present experimental observation that $D_{tt} << D_{rr}$. Thus, although our data at $r > L$ agree well with hydrodynamic expectations consistent with measurements by others (22, 23, 39, 40), we interpret the novel displacement correlations observed in this intermediate regime as signifying a nonhydrodynamic origin.

Consider the dynamical consequences of the above picture. On the relevant intermediate length scales the correlation hole effect implies that it is increasingly unlikely to find pairs of segments on different filaments at separations less than filament length L. The intermolecular segment–segment pair correlation function $g(r) = 1 + h(r)$ of thin, rigid rods is known to be (48)

$$h(r) = \begin{cases} -\frac{1}{18\pi}\left(\frac{\xi}{r}\right)^2\left(1-\frac{r}{L}\right) & d_T < r < L \\ 0 & r \geq L \end{cases}. \qquad [2]$$

Its long-range power law form ("correlation hole") is a distinctive feature of dense liquids of interpenetrating polymers, and for rods $h(r) \sim -1/r^2$ on intermediate length scales. The corresponding intersegment potential of mean force (18) is $W(r) = -k_BT \ln[1 + h(r)] \approx -k_BT\, h(r)$, where the final relation applies because $|h(r)| << 1$. Fig. 4*B* graphically illustrates Eq. **2** for our experimental conditions. To gain some qualitative insight as to what the dynamical consequences might be of such distinctive power law correlations, we compute a simple metric of the number of spatially correlated segments on different rods in a spherical region of radius r centered on a tagged segment by integrating Eq. **2** as $N_{corr}(r) \equiv -\rho_r N 4\pi \int_{d_T}^{r} dx\, x^2 h(x)$. The idea is that $h(r) = g(r) - 1$ is an objective statistical quantification of the deviation from random arrangement in space (on the tube diameter and larger dynamically relevant length scales) of segments on different rods surrounding a tagged segment. The results of this calculation are shown in Fig. 4*B* and one sees that N_{corr} grows strongly with increasing separation, before saturating at $r = L$, which corresponds to the cross-over to random structure. In rough analogy with the phenomenon of critical slowing down of collective dynamics near a phase transition due to the emergence of power law intermolecular static correlations (relevant given Eq. **2**) (49, 50), these emergent structural correlations suggest that dynamic interfilament correlations persist up to distances of approximately the polymer length.

Supporting Information describes mathematical implementation of the above ideas (*SI Theory and Models* and *SI Theoretical Results*). It builds on the theoretical machinery developed previously to successfully relate forces and structure to diffusive dynamical cross-correlations in dense colloidal suspensions (35). The latter applies because use of a rigid-rod model implies that each segment reptates coherently along the tube axis, which allows the dynamical analysis to be performed at the polymer center-of-mass level. The nonhydrodynamic diffusivity, D_{rr}^{non-HD}, can then be derived from knowledge of $h(r)$ and single-rod diffusivity. Worth emphasizing is that this marriage of the collective correlation hole effect with the single tagged polymer tube ideas does not modify in any significant manner the predicted reptation dynamics of single filaments due to topological entanglements (*SI Theoretical Results*, *Single-Filament Diffusivity*, *Numerical Results for Monodisperse Systems*, and *Polydisperse Systems*).

Fig. 4*A* includes our theoretical predictions for $D_{rr}^{non-HD}(r_0)$ and compares them to experiment. Additional calculations of this quantity for other filament lengths and concentrations are given in Figs. S2 and S3. They involve one adjustable parameter, the lower cutoff of the correlation hole behavior of Eq. **2**, which must be proportional to the tube diameter based on our physical picture (i.e., $\lambda\, d_T$). The precise numerical value of the prefactor λ that leads to best theory–experiment agreement is, sensibly, very nearly unity. The theory matches experiments quantitatively up to $r_0 < L \approx 15$ μm within the experimental uncertainty. However, as anticipated, it falls below the experimental data at larger separations because the calculation ignores hydrodynamic effects beyond the macromolecular size. Moreover, correlation hole physics as the origin of collective dynamics does not apply at separations significantly beyond the filament length. This reasonable description of all of the available experimental data over all separations, which employs $D_{rr} = D_{rr}^{HD} + D_{rr}^{non-HD}$, supports both the proposed physical origin of the dynamic cross-correlations in the intermediate time and length scale regime and the assumption that the nonhydrodynamic and hydrodynamic mobility mechanisms are roughly independent. Furthermore, the theoretical predictions are insensitive to biofilament flexibility and depend only weakly on mean filament length over the range relevant to experiments (Fig. S4) and also are insensitive to contour length polydispersity (Fig. S5).

Conclusion

The experimental methods presented here to perform microrheology without use of probe particles may find general use. Using them we have considered time and length scales when entangled polymer filaments are known from the literature to be mechanically soft solids showing a dynamic plateau shear modulus due to spatial localization in two transverse directions (9, 23, 31, 32, 51) yet (as we show here experimentally) the individual molecules continue to display Fickian diffusion of a viscous liquid in the longitudinal direction of the chain contour. In these entangled systems the strongly interpenetrating nature of linear polymers causes the number of correlated "segmental neighbors" on the macromolecular length scale to increase with distance from a tagged polymer out to the filament contour length scale (51). Our analysis of the correlated motion of pairs of entangled polymers, not addressed by the classical tube model, involves considering crowding effects beyond the nearest-neighbor local cages in small-molecule and colloidal liquids.

This paper introduces several physical ideas that may apply beyond the actin biofilaments studied here: (*i*) how cooperative biofilament diffusion deviates from the single-filament behavior averaged within the entanglement time; (*ii*) the notion of emergent "dynamic incompressibility" on intermediate time and length scales, which enables us to model the experimental observations by linking collective dynamics to the correlation hole intermolecular structure of interpenetrating polymers; and (*iii*) the cutoff length scale below which the system fails to behave dynamically like a continuum fluid. We emphasize that this large cutoff far exceeds the physical and entanglement mesh lengths that are traditional to anticipate when considering biofilament or polymer solutions.

Possible extensions to other entangled polymeric systems that exhibit anisotropic dynamics can be considered, all of which generically display the distinctive feature that they respond mechanically as a soft solid on intermediate time and length scales but as a liquid as concerns their anisotropic diffusion. One can anticipate at least three distinct regimes. First, entanglement tubes may be strongly nonoverlapping, $d_T << \xi_m$ and $d_T/\xi_m \propto (\rho_r L^3)^{-1/2}$, a condition that applies to heavily entangled literal rigid-rod polymers such as microtubules and some viruses (52). Second, the entanglement tubes might be close-packed with $d_T \approx \xi_m$ per the semiflexible biopolymer case studied here. Third, the entanglement tubes might be strongly overlapping with $d_T >> \xi_m$, $d_T/\xi_m \propto c^{\Delta}$ (1–3). This condition describes not only solutions of flexible chains under good ($\Delta = 0$) and theta

($\Delta = 1/3$) solvent conditions but also more concentrated solutions and even undiluted melts of entangled chains (1–3). Beyond the questions considered here of dynamical displacement correlations the theoretical issues raised are expected to be relevant to modeling the collective noncontinuum aspects of the mechanical response of entangled polymeric networks of high importance in materials engineering and biological applications, a topic that remains not well understood.

Materials and Methods

Segments and backbones of F-actin were visualized by two-color fluorescence microscopy focused deep into the sample to avoid potential wall effects. Images were collected typically at 10 frames per second for 200 s then analyzed by MATLAB codes written in-house to give trajectories with 10-nm precision. This work treats the segment–segment separation range 0.3–50 μm and time range 0.1–1 s. Details of the experiments and theoretical modeling, and additional results, are provided in *SI Materials and Methods*.

ACKNOWLEDGMENTS. We thank William Brieher (University of Illinois at Urbana–Champaign) for donating the fluorescent-labeled actin. This work was supported by Institute for Basic Science Project IBS-R020-D1 (to S.G.). The theoretical work was supported by US Department of Energy, Division of Materials Science Award DEFG02-07ER46471 (to Z.E.D. and K.S.S.) through the Frederick Seitz Materials Research Laboratory at the University of Illinois at Urbana–Champaign. Experiments were supported by US Department of Energy Award DEFG02-02ER46019 (to B.T., L.J., and S.G.).

1. Rubinstein M, Colby RH (2007) *Polymer Physics* (Oxford Univ Press, New York).
2. Doi M, Edwards SF (1986) *The Theory of Polymer Dynamics* (Clarendon, Oxford).
3. de Gennes PG (1979) *Scaling Concepts in Polymer Physics* (Cornell Univ Press, Ithaca, NY).
4. de Gennes PG (1971) Reptation of a polymer chain in the presence of fixed obstacles. *J Chem Phys* 55:572.
5. Edwards SF (1967) The statistical mechanics of polymerized material. *Proc Phys Soc* 92:9.
6. Likhtman AE (2012) Viscoelasticity and molecular rheology. *Polymer Science: A Comprehensive Reference*, eds Matyjaszewski K, Martin Möller M (Elsevier, Amsterdam), Vol 1, pp 133–179.
7. Wang B, et al. (2010) Confining potential when a biopolymer filament reptates. *Phys Rev Lett* 104(11):118301.
8. Everaers R, et al. (2004) Rheology and microscopic topology of entangled polymeric liquids. *Science* 303(5659):823–826.
9. Käs J, Strey H, Sackmann E (1994) Direct imaging of reptation for semiflexible actin filaments. *Nature* 368(6468):226–229.
10. Nykypanchuk D, Strey HH, Hoagland DA (2002) Brownian motion of DNA confined within a two-dimensional array. *Science* 297(5583):987–990.
11. Harasim M, Wunderlich B, Peleg O, Kröger M, Bausch AR (2013) Direct observation of the dynamics of semiflexible polymers in shear flow. *Phys Rev Lett* 110(10):108302.
12. Broedersz CP, MacKintosh FC (2014) Modeling semiflexible polymer networks. *Rev Mod Phys* 86:995.
13. Ramanathan S, Morse DC (2007) Simulations of dynamics and viscoelasticity in highly entangled solutions of semiflexible rods. *Phys Rev E Stat Nonlin Soft Matter Phys* 76(1 Pt 1):010501.
14. Fetters LJ, Lohse DJ, Richter D, Witten TA, Zirkel A (1994) Connection between polymer molecular weight, density, chain dimensions, and melt viscoelastic properties. *Macromolecules* 27:4639–4647.
15. Chaudhuri P, Berthier L, Kob W (2007) Universal nature of particle displacements close to glass and jamming transitions. *Phys Rev Lett* 99(6):060604.
16. Weeks ER, Crocker JC, Levitt AC, Schofield A, Weitz DA (2000) Three-dimensional direct imaging of structural relaxation near the colloidal glass transition. *Science* 287(5453):627–631.
17. Cavagna A (2009) Supercooled liquids for pedestrians. *Phys Rep* 476:51.
18. Hansen JP, McDonald IR (1986) *Theory of Simple Liquids* (Academic, London).
19. Happel J, Brenner H (1991) *Low Reynolds Number Hydrodynamics* (Kluwer, Dordrecht, The Netherlands).
20. Squires TM, Mason TG (2010) Fluid mechanics of microrheology. *Annu Rev Fluid Mech* 42:413.
21. Starrs L, Bartlett P (2003) One-and two-point microrheology of viscoelastic media. *J Phys Condens Matter* 15:S251.
22. Crocker JC, et al. (2000) Two-point microrheology of inhomogeneous soft materials. *Phys Rev Lett* 85(4):888–891.
23. Gardel ML, Valentine MT, Crocker JC, Bausch AR, Weitz DA (2003) Microrheology of entangled F-actin solutions. *Phys Rev Lett* 91(15):158302.
24. Chen DTN, Wen Q, Janmey PA, Crocker JC, Yodh AG (2010) Rheology of soft materials. *Annu Rev Condens Matter Phys* 1:301–322.
25. Muthukumar M, Edwards S (1983) Screening of hydrodynamic interaction in a solution of rodlike macromolecules. *Macromolecules* 16:1475–1478.
26. Pryamitsyn V, Ganesan V (2008) Screening of hydrodynamic interactions in Brownian rod suspensions. *J Chem Phys* 128(13):134901.
27. Frey E, Kroy K, Wilhelm J (1999) Viscoelasticity of biopolymer networks and statistical mechanics of semiflexible polymers. *Advances in Structural Biology* 5:135–168.
28. Zhou HX, Rivas G, Minton AP (2008) Macromolecular crowding and confinement: Biochemical, biophysical, and potential physiological consequences. *Annu Rev Biophys* 37:375–397.
29. Ellis RJ (2001) Macromolecular crowding: Obvious but underappreciated. *Trends Biochem Sci* 26(10):597–604.
30. Ellis RJ (2001) Macromolecular crowding: An important but neglected aspect of the intracellular environment. *Curr Opin Struct Biol* 11(1):114–119.
31. Dichtl MA, Sackmann E (2002) Microrheometry of semiflexible actin networks through enforced single-filament reptation: Frictional coupling and heterogeneities in entangled networks. *Proc Natl Acad Sci USA* 99(10):6533–6538.
32. Hinner B, Tempel M, Sackmann E, Kroy K, Frey E (1997) Entanglement, elasticity and viscous relaxation of actin solutions. *Phys Rev Lett* 81:2614–2617.
33. Wang B, Anthony SM, Bae SC, Granick S (2009) Anomalous yet Brownian. *Proc Natl Acad Sci USA* 106(36):15160–15164.
34. Anthony S, Zhang L, Granick S (2006) Methods to track single-molecule trajectories. *Langmuir* 22(12):5266–5272.
35. Dell ZE, Tsang B, Jiang L, Granick S, Schweizer KS (2015) Correlated two-particle diffusion in dense colloidal suspensions at early times: Theory and comparison to experiment. *Phys Rev E Stat Nonlin Soft Matter Phys* 92(5):052304.
36. Schmidt CF, Baermann M, Isenberg G, Sackmann E (1989) Chain dynamics, mesh size, and diffusive transport in networks of polymerized actin: A quasielastic light scattering and microfluorescence study. *Macromolecules* 22:3638–3649.
37. Morse DC (2001) Tube diameter in tightly entangled solutions of semiflexible polymers. *Phys Rev E Stat Nonlin Soft Matter Phys* 63(3 Pt 1):031502.
38. Li G, Tang JX (2004) Diffusion of actin filaments within a thin layer between two walls. *Phys Rev E Stat Nonlin Soft Matter Phys* 69(6 Pt 1):061921.
39. Ziemann F, Rädler J, Sackmann E (1994) Local measurements of viscoelastic moduli of entangled actin networks using an oscillating magnetic bead micro-rheometer. *Biophys J* 66(6):2210–2216.
40. Koenderink GH, Atakhorrami M, MacKintosh FC, Schmidt CF (2006) High-frequency stress relaxation in semiflexible polymer solutions and networks. *Phys Rev Lett* 96(13):138307.
41. Zwanzig R (2008) *Nonequilibrium Statistical Mechanics* (Oxford Univ Press, New York).
42. Gotze W (2008) *Complex Dynamics of Glass-Forming Liquids: A Mode-Coupling Theory* (Oxford Univ Press, Oxford).
43. Sussman DM, Schweizer KS (2011) Theory of correlated two-particle activated glassy dynamics: General formulation and heterogeneous structural relaxation in hard sphere fluids. *J Chem Phys* 134(6):064516.
44. Sussman DM, Schweizer KS (2012) Space-time correlated two-particle hopping in glassy fluids: Structural relaxation, irreversibility, decoupling, and facilitation. *Phys Rev E Stat Nonlin Soft Matter Phys* 85(6 Pt 1):061504.
45. Yamamoto U, Schweizer KS (2013) Spatially dependent relative diffusion of nanoparticles in polymer melts. *J Chem Phys* 139(6):064907.
46. Kirkpatrick TR, Wolynes PG (1987) Connections between some kinetic and equilibrium theories of the glass transition. *Phys Rev A Gen Phys* 35(7):3072–3080.
47. Yamamoto U, Schweizer KS (2011) Theory of nanoparticle diffusion in unentangled and entangled polymer melts. *J Chem Phys* 135(22):224902.
48. Marques C, Fredrickson G (1997) Rigid Gaussian chains I: The scattering function. *J Phys II* 7:1805–1816.
49. Goldenfeld N (1992) *Lectures on Phase Transitions and the Renormalization Group* (Westview, Boulder, CO).
50. Hohenberg PC, Halperin BI (1977) Theory of dynamic critical phenomena. *Rev Mod Phys* 49:435.
51. Guenza MG (2014) Localization of chain dynamics in entangled polymer melts. *Phys Rev E Stat Nonlin Soft Matter Phys* 89(5):052603.
52. Brangwynne CP, MacKintosh FC, Weitz DA (2007) Force fluctuations and polymerization dynamics of intracellular microtubules. *Proc Natl Acad Sci USA* 104(41):16128–16133.
53. Deutch J, Oppenheim I (1971) Molecular theory of Brownian motion for several particles. *J Chem Phys* 54:3547.
54. Evans GT, Kivelson D (1986) Pair diffusion at close range in liquids. *J Chem Phys* 85:7301.
55. Guenza M (1999) Many chain correlated dynamics in polymer fluids. *J Chem Phys* 110:7574.
56. Vineyard GH (1958) Scattering of slow neutrons by a liquid. *Phys Rev* 110:999.
57. de Gennes PG (1959) Liquid dynamics and inelastic scattering of neutrons. *Physica* 25:825.
58. Edelstein-Keshet L, Ermentrout GB (1998) Models for the length distributions of actin filaments: I. Simple polymerization and fragmentation. *Bull Math Biol* 60(3):449–475.